Materials Advances

ROYAL SOCIETY OF CHEMISTRY

PAPER

View Article Online
View Journal | View Issue

Cite this: *Mater. Adv.*, 2025, 6, 2549

Orthogonal effect of pyrene–porphyrin conjugates on the detection of volatile organic compounds under UV and visible light illumination through surface photovoltage†

Prasanth Palanisamy,[a] Mageshwari Anandan,[a] Sheethal Sasi,[b] Arbacheena Bora,[b] Sarath Kumar Chedharla Balaji,[c] Rence P. Reji,[c] Yoshiyuki Kawazoe,[d] Kommineni Kalyani,[f] Surya Velappa Jayaraman,*[cd] Yuvaraj Sivalingam[be] and Venkatramaiah Nutalapati*[a]

In this work, we have developed two modular compounds featuring pyrene at the meso position of the freebase porphyrin (H_2PyP) and its complex with Zn (ZnPyP). Both compounds exhibited a unique energy transfer process due to the orthogonal pyrene units, demonstrating that appreciable electronic interactions existed between the peripheral units and the porphyrin π-system. These compounds were found to behave as strong donor materials in solid-state thin films. Detailed photophysical properties and excited-state interactions in the gas phase were modulated through surface photovoltage measurements using the scanning Kelvin probe (SKP) technique. These interactions were explored towards the detection of different volatile organic compounds (VOCs) (ethanol, acetone, 1-hexanol, triethylamine, nonanal, and acetonitrile) under dark, UV and visible light illuminations. H_2PyP and ZnPyP showed n-type behaviour with high selectivity towards 1-hexanol under UV light illumination, while under visible light illumination, ZnPyP exhibited n-type behaviour and H_2PyP showed p-type behaviour. The response and recovery studies demonstrated that H_2PyP and ZnPyP showed unprecedented selectivity towards 1-hexanol by altering their p- and n-type behaviour. H_2PyP exhibited a high photovoltage response of 93% for an exposure of 17 s with a recovery rate of 23% in 5 s, while ZnPyP showed 97% in 2 s with a recovery rate of 55% in 116 s under UV light. The unique response of H_2PyP and ZnPyP to 1-hexanol could be attributed to donor–donor interactions and intermolecular hydrogen bonding at the central core, as well as the variations in the energy transfer process. Furthermore, density functional theory studies revealed that the binding interactions of H_2PyP and ZnPyP with VOCs showed a greater affinity for alcohol vapours compared to other compounds.

Received 11th December 2024,
Accepted 24th February 2025

DOI: 10.1039/d4ma01228c

rsc.li/materials-advances

1. Introduction

Volatile organic compounds (VOCs) are abundant in the environment and pose substantial risks to human health and safety.[1] The identification of VOCs is essential for a wide range of purposes, such as monitoring the environment, controlling industrial processes, and ensuring national security.[2–5] Among the various toxic VOCs, 1-hexanol and nonanal are used as biomarkers in fish, and monitoring the emission of these VOCs indicates the freshness of the fish.[6,7] Conventional techniques for detecting VOCs typically require sophisticated equipment and may have limitations in terms of sensitivity or specificity.[8] The scanning Kelvin probe (SKP) technique is a highly sensitive and non-invasive method for detecting VOCs.[9] It measures variations in the contact potential difference (CPD) between a reference probe and a sample surface, making it a powerful tool

[a] *Functional Materials Laboratory, Department of Chemistry, Faculty of Engineering and Technology, SRM Institute of Science and Technology, Kattankulathur 603203, India. E-mail: nvenkat83@gmail.com, venkatrv1@srmist.edu.in*
[b] *Laboratory of Sensors, Energy and Electronic Devices (Lab SEED), Department of Physics and Nanotechnology, SRM Institute of Science and Technology, Kattankulathur 603203, Tamil Nadu, India*
[c] *Novel, Advanced, and Applied Materials (NAAM) Laboratory, Department of Physics and Nanotechnology, SRM Institute of Science and Technology, Kattankulathur 603203, Tamil Nadu, India. E-mail: suryaj@srmist.edu.in*
[d] *New Industry Creation Hatchery Centre (NICHe), Tohoku University, Aoba-ku, Sendai 980-8579, Miyagi, Japan*
[e] *Computer, Electrical and Mathematical Sciences and Engineering Division (CEMSE), King Abdullah University of Science and Technology (KAUST), Thuwal 23955-6900, Kingdom of Saudi Arabia*
[f] *Department of Chemistry, RVR & JC College of Engineering, Guntur, Andhra Pradesh 522019, India*

† Electronic supplementary information (ESI) available. See DOI: https://doi.org/10.1039/d4ma01228c

for VOC sensing. This method is especially beneficial for detecting VOCs due to its non-invasive approach and provides precise measurements in real time without having a direct contact with the sample, thus minimizing the risk of contamination and interference.[10] Incorporation of SKP with cutting-edge materials, such as organic semiconductors and hybrid systems, has increased its efficiency in detecting VOCs. The utilization of materials possessing customized electronic characteristics and elevated surface reactivity can enhance the sensitivity and selectivity of the SKP technique. It can detect a broad spectrum of VOCs at low levels and under varying environmental circumstances.[11]

Porphyrins play a vital role in augmenting the capabilities of SKP techniques for detecting VOCs. Due to their distinctive chemical and electronic properties, they are exceptionally efficient as sensor materials.[12] They possess a substantial surface area and exhibit significant reactivity owing to their conjugated ring systems.[13] The high surface area increases their capacity to adsorb VOCs, resulting in more noticeable alterations in the chemiluminescence peak detected by SKP as the n-type or p-type behaviour.[14] The interaction between the porphyrins and VOCs can result in detectable changes in the charge transfer processes, enabling the identification of even very low concentrations of VOCs.[15] By modifying the metal centres or substituent groups, one can precisely adjust the electronic characteristics of porphyrins. The ability to adjust and control the properties of porphyrin-based sensors enables the creation of sensors that have specific attractions to various VOCs.[16] By carefully choosing the porphyrin derivatives, sensors can be enhanced to detect specific VOCs, enhancing the selectivity and minimizing interference from other substances.[17] The orientation of substituents at the meso position with an orthogonal approach exhibits an efficient intramolecular electron/energy transfer process through favourable extended π–π electronic interactions for effective long-lived ion pair states. These configurations have the potential to improve singlet energy transfer, which is crucial for solar energy conversion and photodynamic treatment applications.[18] The induction of rigid fused aromatic structures like pyrene at the meso position of the porphyrin molecules improves the π–π stacking interactions in these systems and increases the mobility of charge carriers due to the orthogonal effect.[19]

Incorporating meso-substituted porphyrins and metalloporphyrin into the SKP-based sensors becomes an excellent technique for detecting volatile organic compounds (VOCs) in real-time with high sensitivity.[20] Extended conjugation offers a huge opportunity to construct organic semiconductors based on the D–D (Donor–Donor) framework because of the pervasiveness of the charge transfer process in the D–D molecules. Marappan *et al.* synthesised naphthalene-attached DPP molecules functionalized with ZnO nanostructures at different pH values (pH 9 and 11) in terms of gas adsorption, which exhibited a greater photo response towards 1-hexanol at pH 11.[21] Our group has recently reported the polymorphism-driven gas adsorption on the naphthalic imide-decorated phenothiazine unit surface, which shows that preferential photo response toward VOCs is induced by the surface morphology and interaction sites.[22] Elakia *et al.* investigated the gas-sensing properties of pyrene molecules with the –COOH functionality coated on multi-walled carbon nanotubes. The study reported that pyrene coupled to –COOH exhibits powerful intermolecular H-bonding mediated by the D–A contact, resulting in good selectivity for triethylamine with favourable response and recovery.[23] As a biomarker for liver diseases, the gas adsorption impacts on the surface of a phthalocyanine-coated TiO_2 thin film were demonstrated by Sivalingam *et al.* The VOC that patients with liver illnesses exhale through their breath is triethylamine, and the functionalized thin film demonstrated improved sensitivity and selectivity for triethylamine detection.[24] Reji *et al.*, on the other hand, published VOC adsorption tests on Fe(II) phthalocyanine and metal-free samples, which demonstrated solid-state J-aggregation. Fe(II) phthalocyanine displays a selective photoresponse to nonanal and 1-hexanol under dark and visible light illumination, respectively, in contrast to metal-free phthalocyanine.[25] By using DFT, Wang *et al.* examined the ground-state molecular structures, electron distributions, and UV spectra features of octaethyl porphyrins with various central metals (M-OEP, M = Ni, V, O, Cu, and Co). The results demonstrate a good agreement between the experimental value and the computational structure parameters of metalloporphyrins.[26] Gawas *et al.* reported the substituent effect on stimuli-responsive donor–acceptor framework-based 2-thiohydantoins for nonanal vapour monitoring. The structure–function relationship examined in this work may offer important insights for the creation of highly effective gas sensors and also show the effect of extended π-conjugation on 2-thiohydantoins to a strictly defined volatile organic compound detection by surface photovoltaics.[27,28] Sasi *et al.* developed a boron-doped diamond (BDD) surface functionalized with 5-(4-carboxyphenyl) triphenyl porphyrins, and gas adsorption was investigated at room temperature. Using the SKP system, the surface potential distribution caused by the adsorption of VOCs under visible light illumination conditions was examined, following the structural and morphological characterisations of the porphyrin-functionalized BDD surface and the bare BDD surface. Under visible light, the porphyrin-functionalized BDD thin film showed a selective response towards triethylamine.[29] Marappan *et al.* investigated the capacity of vertically grown ZnO NRs functionalized with triphenylamine (TPA) derivatives for VOC sensing. Under dark conditions, the functionalized ZnO NRs exhibit superior gas sensitivity towards nonanal, as demonstrated by the SKP experiments. It shows excellent adsorption towards nonanal under light illumination.[30] Based on the literature reports, the organic material synthesised in this work could be suitable for gas adsorption studies to determine novel structure–reactivity relationships and provide new avenues for the selective detection of VOCs.

In this study, we describe the synthesis and photophysical properties of pyrene-tethered meso-substituted freebase porphyrin and its Zn(II) complex to ascertain the role of the orthogonal effect of molecular ensembles on the gas adsorption behaviour with different VOCs by changing the surface photovoltages. The change in the work function of the material by the adsorption of VOCs on the sample surface due to physisorption or chemisorption was monitored under the dark, UV and visible light illumination. Under UV and visible light illumination, the highest photovoltage

response was exhibited by 1-hexanol, followed by nonanal. By modifying the D–D design with different donors that overlap with higher electron densities, selectivity to VOCs is achieved, along with quick recovery. The detailed mechanistic investigation of the photoresponse behaviour is further analysed in terms of the binding interactions using density functional theory (DFT).

2. Materials and methods

All the A. R grade chemicals and solvents were procured from Sigma Aldrich and Avra Chemicals Ltd, India, and used directly without additional purification. Fourier-transform infrared (FT-IR) spectra were recorded using Shimadzu IR Tracer-100 under the KBr mode. NMR (^{1}H and ^{13}C) spectra were measured at 300 MHz with TMS as the internal reference. ESI-MS analysis was carried out in an LC–MS 2020 system equipped with an LC10ADVP binary pump (Shimadzu, Japan). An Agilent Cary 60 UV-Vis spectrometer was used to record the absorption spectra in both thin films and solutions. The steady-state fluorescence spectra of thin films were measured in an FLS 1000 photoluminescence spectrometer. The contact potential difference (CPD) measurements were performed using a surface photovoltage module using a 2 mm vibrational gold tip operating at 78.3 Hz in the Scanning Kelvin Probe System (SKP) (SKP5050, KP Technology Ltd, UK). The High-Resolution Transmission Electron Microscope (HR-TEM) images were obtained using JEOL 2100 transmission electron microscope. High-Resolution Scanning Electron Microscope (HR-SEM) images were obtained from a Thermo Scientific Apreo S spectrometer. Ground state geometry optimization was carried out in the Gaussian16 software with a basis set of 6-311++G (d,p)/LANL2DZ with hybrid functions in B3LYP and visualization was made with Gauss View 5.2 suit software.

2.1. Synthesis

2.1.1. Synthesis of meso-5,10,15,20-tetrakis(pyren-1-yl)porphyrin (H_2PyP). In a 500 mL round base flask, distilled propionic acid (200 mL) and pyrrole (0.583 mL, 8.6 mmol) were taken. To this, pyrene-1-carbaldehyde (2 g, 8.6 mmol) was added, and the reaction mixture was kept for refluxing at 150 °C under air conditions. The progress of the reaction was monitored by TLC chromatography. The reaction mixture was cooled to room temperature and kept in the refrigerator overnight. The obtained black color precipitate was filtered off under a vacuum and washed thoroughly with water and methanol. Finally, a silica gel column was employed to purify the product using hexane : chloroform as eluent (20 : 80, v/v%). Yield. 2.3%. ^{1}H NMR (300 MHz, $CDCl_3$) (ppm): δ 8.86–8.75 (m, 3H), δ 8.46–8.42 (m, 10H), δ 8.34–8.25 (m, 12H), δ 8.07–7.99 (m, 10H), δ 7.74–7.69 (m, 4H), δ 7.64–7.60 (m, 2H) δ 7.58–7.46 (m, 3H) and δ −1.96 (s, 2H, N–H). ^{13}C NMR (75 MHz) δ (ppm): 131.71, 131.47, 130.79, 128.06, 127.64, 126.29, 125.32, 125.02, 122.81 and 122.78. ESI-MS: calcd for $C_{84}H_{46}N_4$ (m/z): 1110.3722; found: 1134.2000 $[M + Na]^+$.

2.1.2. Synthesis of meso-5,10,15,20-tetrakis(pyren-1-yl)porphyrinato zinc(II) (ZnPyP). Freebase porphyrin (H_2PyP) (70 mg, 0.062 mmol) was dissolved in THF (5 mL) and the solution was purged with nitrogen for 10 min. A solution of $Zn(OAc)_2$ (20.7 mg, 0.094 mmol) in MeOH (3 mL) was added to the H_2PyP solution, and the reaction mixture was stirred overnight. The solvent was removed under vacuum and purified through a silica gel column, giving a brown solid. Yield. (65 mg, 87%). ^{1}H NMR (300 MHz, $CDCl_3$) (ppm): δ 8.89–8.76 (m, 3H), δ 8.51–8.45 (m, 7H), δ 8.35–8.33 (m, 7H), δ 8.29–8.24 (m, 5H), δ 8.07–8.00 (m, 5H), δ 7.99 (s, 1H), δ 7.75–7.67 (m, 6H) and δ 7.62–7.45 (m, 3H) ^{13}C NMR (75 MHz, $CDCl_3$) (ppm): δ 151.31, 132.63, 132.52, 132.47, 131.75, 131.30, 130.82, 127.90, 127.66, 126.21, 125.47, 125.47, 125.19, 124.65, and 122.661. ESI-MS: calcd for $C_{84}H_{46}N_4$ (m/z): 1174.6550; found: 1176.2500 $[M + 2H]^+$.

2.2 Scanning Kelvin probe measurements for gas adsorption studies

To study the gas adsorption properties of the samples, the SKP measurements were carried out. The fluorine-doped tin oxide (FTO) coated glass substrates (~15 Ω) with a dimension of 2 × 2 cm^2 were washed with a soap solution, distilled water, acetone, and ethanol in an ultra-sonicated bath for 30 minutes at 55 °C after which it was spin-coated with H_2PyP and ZnPyP. The coated films were dried for 4 h at room temperature, and subsequently, the gas adsorption studies were performed under the SKP module. To measure the changes in the photovoltage of H_2PyP and ZnPyP upon exposure to different VOCs under dark and light conditions, the measurements were performed in a closed chamber at ambient temperature (~25 °C). In order to investigate the effect of light impact on the gas adsorption behaviour, two different light sources, a quartz tungsten halogen (QTH) lamp as a visible light source and long UV light (365 nm), were used as irradiation sources. Initially, the measurements were performed under the air medium as a reference. Then, different VOCs with varied vapour pressures like acetone, ethanol, 1-hexanol, acetonitrile, nonanal, and triethylamine were chosen to ascertain their donor and acceptor characteristics. Concentration-based studies were not done in the SKP chamber. Instead, a constant amount (~20 mL) of each VOC was exposed and allowed to vapourize inside the chamber at 25 °C for a constant time (~10 minutes), after which the measurements were performed. For maintaining the volatility of the used VOCs, the obtained CPD values were divided by the corresponding values of saturated vapour pressures (SVP) of each VOCs. The results were divided by the saturated vapour pressure (SVP) of each VOC at 25 °C. The SVP was calculated using Antoine's eqn (1) at 25 °C.

$$\log(\mathrm{Pi}) = A - \frac{B}{C + T} \quad (1)$$

where A, B and C are Antoine's parameters, Pi is the vapour pressure of VOC and T is the temperature (25 °C).

3. Results and discussions

The freebase porphyrin (H_2PyP), having four pyrene units at the meso position, was synthesized using Adler's method through a reflux condensation reaction between pyrrole and 1-pyrenecarboxaldehyde in a propionic acid medium for 2 h

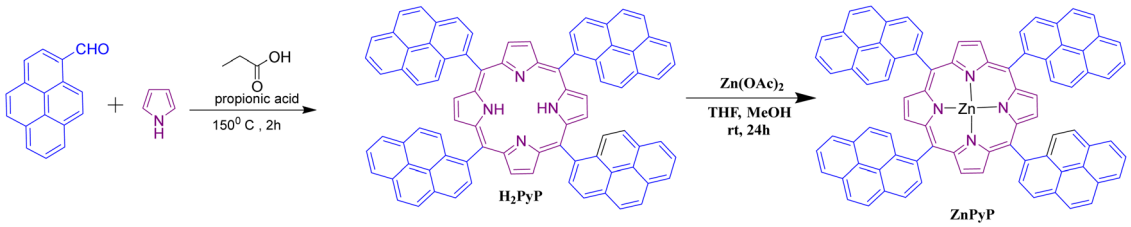

Scheme 1 Synthesis routes for H_2PyP with ZnPyP.

(Scheme 1). Column chromatography was used to isolate, purify and characterize the target compound. Further, the metalation of H_2PyP with $Zn(OAc)_2$ was carried out in THF and methanol to obtain ZnPyP with an 80% yield.[31] The FT-IR spectrum of H_2PyP reveals a distinctive vibrational peak at 3307.45 cm^{-1} corresponding to N–H stretching, peak at 1583 cm^{-1} indicating the C=C bonds, another peak at 1453 cm^{-1} representing the C=N bonds, a band at 1343 cm^{-1} for the C–N bonds, a signal at 1052 cm^{-1} associated with the aromatic structures and a peak at 961 cm^{-1} attributed to aromatic C–H bonds. Upon metalation, the C=C band shifts to 1586 cm^{-1}, while the C=N and C–N bands shift to 1334 cm^{-1} and 1250 cm^{-1}, respectively (Fig. S1, ESI†). The ^1H NMR spectrum of H_2PyP showed a singlet signal due to the –NH protons at a highly shielded region at δ −1.96 ppm, and the aromatic β-pyrrole and meso-pyrenyl protons of H_2PyP resonate in the aromatic region at δ 8.86–7.46 ppm (Fig. S2 and S3, ESI†). For ZnPyP, the singlet signals attributed to the –NH protons disappeared, while the aromatic region remained between δ 8.89–7.45 ppm (Fig. S4 and S5, ESI†). The ESI-MS spectra of H_2PyP and ZnPyP showed molecular ion peaks at m/z 1134.2000 $[M + Na]^+$ and 1176.2500 $[M + 2H]^+$, respectively, which corroborate the final desired compounds (Fig. S6 and S7, ESI†).

Fig. 1(a) shows the absorption spectra of the H_2PyP and ZnPyP thin films coated on the quartz substrate. The H_2PyP thin film showed a broad Soret band absorption at 450 nm along with four Q-band patterns in the 520–660 nm region. In addition, we observed vibronic absorption bands at 235 nm ($S_0 \rightarrow S_4$) and 264 nm ($S_0 \rightarrow S_3$), and the broad absorption at 320–330 nm region corresponds to the $S_0 \rightarrow S_2$ transitions of pyrene.[32,33] The Soret band shows strong red-shifted absorption in comparison with H_2TPP due to the extended conjugation of pyrene. The ZnPyP thin film shows a Soret band at 450 nm along with the Q bands at 566 and 633 nm. The four Q-band patterns changing to the two-band pattern confirms the metalation at the central core. The absorption of pyrene in the ZnPyP thin film is much broader and red-shifted in comparison with the H_2PyP thin film. The absorption spectra in thin films are found to be broader and red-shifted than in the solution by ~5–10 nm shifts due to their strong molecular arrangements (Fig. S8, ESI†). Pyrene shows different emission behaviour, with the monomer emission centred at 383 nm and the excimer emission at 470 nm. The free base porphyrin (H_2TPP) shows two band emissions at 652 and 715 nm originating from the $S_1 \rightarrow S_0$ transition. The steady-state emission spectra of the H_2PyP thin film at different excitation wavelengths were carried out to ascertain the emission behaviour due to different modes of conjugation. On excitation of the H_2PyP thin film at λ_{ex} = 330 nm, we observed three different broad emission bands centred at 438, 452 and 469 nm, along with an intense broad emission at 650–750 nm region, which is attributed to the $S_1 \rightarrow S_0$ emission of the Soret band. The emission peak at 469 nm corresponds to the emission features of the excimer emission. The observed red shift in comparison to pristine compounds indicates the increase in the conjugation of pyrene due to the orthogonal orientation similar to the absorption spectra. The spectral overlap of the pyrene emission and Soret band absorption indicates the intramolecular energy transfer from the peripheral pyrene to the H_2PyP thin film. A similar observation

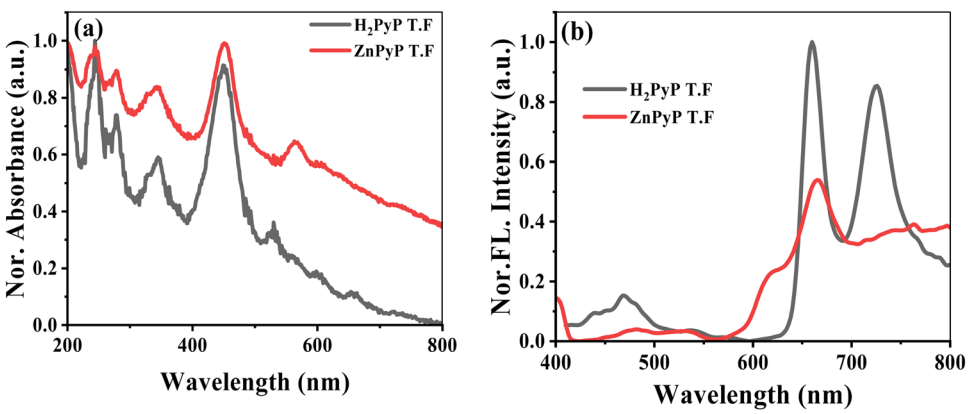

Fig. 1 Absorption spectra of H_2PyP and ZnPyP coated on a quartz substrate (a). (b) Emission spectra of H_2PyP and ZnPyP thin films upon excitation at λ_{ex} = 330 nm.

was made for the H_2PyP thin film dissolved in chloroform solution (Fig. S8, ESI†). Fig. 1(b) shows the emission spectra of the ZnPyP thin film at different excitation wavelengths. Upon excitation at 330 nm, the monomer emission is more predominant than the excimer emission, and the energy transfer process is more prominent for the H_2PyP than ZnPyP. It could arise due to the orientation of pyrene units at the meso position and variations in the planarity (Fig. S9, ESI†).

The surface topology, microstructure and roughness of thin films were analysed through HR-SEM and HR-TEM, as shown in Fig. 2. Thin films were developed by dissolving both compounds in a chloroform solvent with a concentration of 5 mg/mL at room temperature. The films are fabricated by spin coating and then annealing up to 100 °C for 30 min for better self-assembly. The resulting films are homogenous with maximum surface coverage. The scanning electron microscopic (SEM) analysis is carried out to determine the self-assembly characteristics of the active layer. The large planar nature of the porphyrin core, along with pyrene units, tends to undergo aggregation behaviour and results in the formation of large spherical aggregates on the surface (Fig. 2(a)). ZnPyP exhibited agglomerates with small spherical particles resembling nano-flowers (Fig. 2(b)).[34]

The HR-TEM images of H_2PyP (Fig. 2(c)) show bright images with crystalline behaviour indicated by the selected area electron diffraction (SAED) pattern. This behaviour is found to decrease in ZnPyP (Fig. 2(d)). The inter-planar distances were measured to be 0.25 Å. The uniform distribution of the thin film surface morphology suggests that the compounds self-assembled due to strong intermolecular interactions with the energy transfer process, and variation in the surface morphology tailored us to study the gas phase adsorption interactions with VOCs.

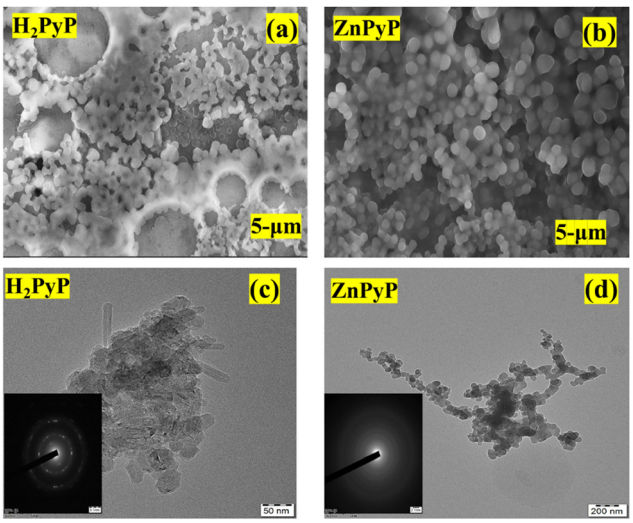

Fig. 2 HR-SEM images of (a) H_2PyP and (b) ZnPyP; high-resolution transmittance electron microscopy images of H_2PyP (c) showing the overall picture of the agglomerated structure, with the inset showing the SAED pattern of polycrystalline H_2PyP; and (d) ZnPyP showing the agglomerated carbon layer, with the inset showing the SAED pattern of amorphous ZnPyP.

To understand the gas adsorption phenomenon, the SKP studies were performed to measure the change in the photovoltage of H_2PyP compared to ZnPyP upon exposure to different VOCs under UV and visible light conditions. Scanning the surface facilitates the verification of the quality of the applied layer, ensuring consistent functionality, including uniform sensor response and electrical conductivity. The uniform CP value throughout the SKP map signifies that the surface exhibits relative homogeneity in its electronic properties, which is advantageous for specific materials, including thin films utilized in optoelectronics. Moreover, reproducible and consistent CP values across the surface validate the stability and accurate calibration of the SKP setup. The 3D raster scanning of the surface helps understand the homogeneity of a certain area of the surface upon VOC adsorption, whereas the single-point CPD measurements only give information about a particular point above which the probe vibrates. A 2 mm diameter gold tip was used as a reference tip, and the alteration in the CPD was recorded under dark conditions and both sources of light. The vibrational frequency of the tip is 78.3 Hz. The gold tip is placed above the surface of the sample. An electrostatic force (F_ω) is felt when the gold tip and sample surface are close together; F_ω is given by the following equation:[35]

$$F_\omega = \frac{-\partial C}{\partial V}(V_{\text{off}} - V_s)V_{\text{ac}} \sin \omega t \quad (2)$$

The CPD is estimated based on the surface potential (V_s), while the electrostatic force (F_ω) between the gold tip and the sample is negated. Utilising an external voltage (V_{off}) through a feedback loop, this surface potential is nullified. A standard-grade gold sample is used to scale the Au tip prior to each measurement. The interplay between the organic molecules and the gaseous environment is calculated based on the changing CPD values. According to the electron-donating or electron-accepting nature of the VOCs involved, the CPD of the samples was assessed with exposure to six different VOCs. All of the samples were initially compared to those in air medium. The photogenerated electrons are released as a result of organic samples being exposed to light illumination. As the measurements were not carried out by varying the VOC concentrations, the results were normalized using the SVP (eqn (1)) of each VOC at 25 °C to compare the volatility of the VOCs.

As shown in Fig. 3(a), an SKP experimental setup was used to quantify changes in surface photovoltages to examine the gas adsorption characteristics of H_2PyP and ZnPyP. The CPD values of H_2PyP and ZnPyP in VOCs under dark conditions are given in Fig. 3(b) and (c), respectively, which gives the distinction between the interactions of molecules to each VOC. Fig. 3(d) represents the normalized CPD measured for the H_2PyP and ZnPyP molecules with respect to air under the dark medium for different VOC environments. These scatter plots clearly portray the selectivity of the molecules towards 1-hexanol vapours, which is followed by the nonanal response. From the raster scanned images of ZnPyP under air and 1-hexanol media, it is evident that a higher response is obtained for ZnPyP in comparison with H_2PyP (Fig. 3(e)). The pyrene tetratopic ligands

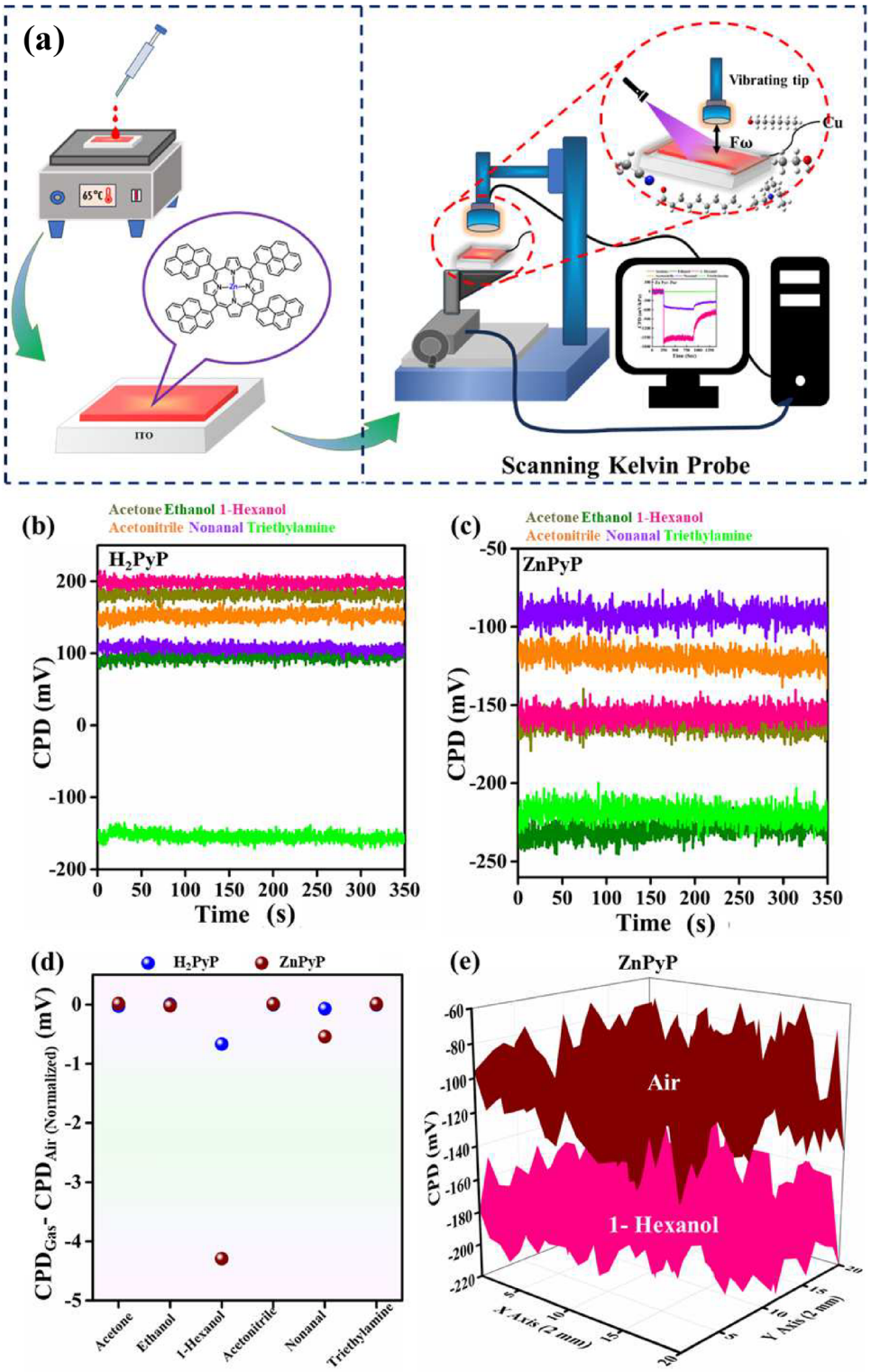

Fig. 3 (a) Schematic of the SKP device used in the present work. Time evolution of the CPD signal under exposure to various VOCs in the dark for (b) H_2PyP and (c) ZnPyP. (d) Normalized CPD plots for VOCs with respect to air for the samples. (e) 3D raster scan image under ambient air and 1-hexanol for ZnPyP.

(PTL) functionalized multiwalled carbon nanotubes (MWCNTs) under light and illumination conditions upon exposure with triethylamine (TEA) vapours exhibit acid–base interactions through a photoinduced electron transfer process.[23] In the same case, pyrene-coated zinc oxide nanorod showed a good response to triethylamine.[36] In contrast, the pyrene-appended porphyrin

derivatives show a higher response through the energy transfer process to 1-hexanol under dark and air conditions.

Fig. 4(a) describes the surface photovoltage (SPV) of H_2PyP and ZnPyP. SPV does not show any significant change until a threshold value of $\sim$12 mW cm^{-2} is reached, which arises due to the insufficient concentration of photogenerated charge carriers due to the lower intensity of light that is not prominent enough to introduce the band bending effect. Once the threshold is crossed, SPV increases in a linear pattern in ZnPyP, showing the highest altitude under air medium. Upon the VOCs exposure, the highest slope is observed in 1-hexanol for both compounds (Fig. S10, ESI†). The CPD values in the dark medium for the gases tested are given in Table 1.

The slope obtained from the SPV plot is −1.5 mV per decade, −1.07 mV per decade, −2.21 mV per decade, −0.57 mV per decade, −1.95 mV per decade and −0.57 mV per decade for the H_2PyP and −0.11 mV per decade, −0.17 mV per decade, −1.11 mV per decade, −0.49 mV per decade, −0.995 mV per decade, −0.37 mV per decade for ZnPyP for acetone, ethanol, 1-hexanol, acetonitrile, nonanal, triethylamine, respectively. An empirical formula was utilised to understand the direct proportionality relationship between the magnitude of the generated surface photovoltage and the degree of brightness of the light, which is as follows.[37,38]

$$\mathrm{SPV} = \frac{\eta k T}{e} \ln(BI). \quad (3)$$

I is the fluctuating light intensity, η and B are the proportionality constants. To verify the proportionality constant as a measure of the defect state present in the nanostructure, the fitted data is considered. The greater the value of the slope, the greater the number of defects in the structure. Upon exposure to 1-hexanol, we observed the highest η value of −5.09 and −10.09 for H_2PyP and ZnPyP, respectively. The η values of other VOCs are tabulated in (Table S1 and Fig. S10, ESI†). Fig. 4(b) represents the resultant CPD that arises when the organic samples are switched between dark and light conditions, both UV and visible, in ambient air. The noise value of the CPD signals is addressed by the error bar. ZnPyP exhibits an enhanced CPD under UV light exposure when compared to H_2PyP, although neither molecule exhibits significant CPD changes with exposure to visible light or in the dark. This reaction is brought on by the absorption of the porphyrin component, which extends into the visible spectrum, and the intensification under UV light is caused by the absorption of the pyrene component in the ultraviolet spectrum of H_2PyP and ZnPyP. However, a striking difference in

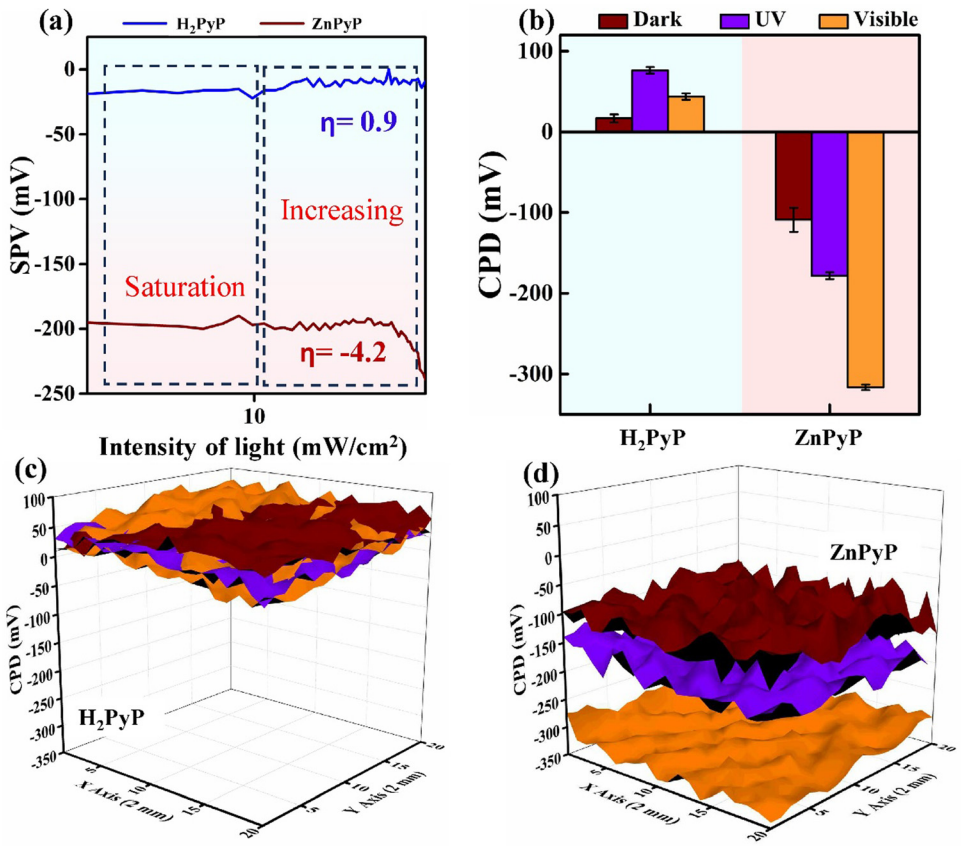

Fig. 4 (a) Surface photovoltage changes of H_2PyP and ZnPyP in air. (b) CPD changes from dark to UV and visible light illumination in H_2PyP and ZnPyP. 3D raster scan images under dark, UV and visible light illumination in (c) H_2PyP and (d) ZnPyP under ambient air.

Table 1 Change in the CPD values in the dark medium for H_2PyP and ZnPyP under exposure to different VOCs

	CPD values under the dark medium (mV)					
Molecular substrate	Acetone	Ethanol	1-Hexanol	Acetonitrile	Nonanal	Triethylamine
H_2PyP	58.37	113.84	25.20	20.56	89.71	−58.84
ZnPyP	−119.76	−93.91	−152.08	−132.95	−92.99	−138.51

the CPD value results from the presence of greater absorption in the UV and visible regions as well as the presence of strong red-shifted excimers.[23] Fig. 4(c) and (d) display the 3D raster scanned images under the dark, UV and visible light exposure of H_2PyP and ZnPyP, respectively.

The switching in the CPD response upon exposure to UV radiation after maintaining the sample in the dark environment under various VOC environments is shown in Fig. 5. From Fig. 5(a) and (b), 1-hexanol demonstrated the largest photovoltage response when exposed to UV light, followed by nonanal. Upon exposure to other gases, the molecules showed no significant changes in the CPD values. H_2PyP exhibited a n-type behaviour towards saturated vapours of 1-hexanol and nonanal, same behaviour is observed in the case of ZnPyP. Overall, ZnPyP and H_2PyP showed better selectivity towards 1-hexanol, followed by nonanal, acetone, and ethanol, as compared to the other gases. In contrast to these two gases, exposure to other gases (*viz.* acetone, ethanol, triethylamine, acetonitrile) does not produce any remarkable change in its CPD. Upon exposure to pure vapours of 1-hexanol, the H_2PyP exhibited an n-type behaviour similar to ZnPyP. The behaviour of the H_2PyP in a 1-hexanol environment changes as the light source is switched from a UV source to quartz tungsten halogen (QTH) as a visible light source with an intensity of 70 mW cm^{-2} (Fig. 5(d) and (e)). For both the compounds, 1-hexanol and nonanal vapours exhibit the highest levels of selectivity through the CPD change on dark-to-light illumination. ZnPyP showed the strongest interaction with gas molecules upon exposure to UV light. However, the ZnPyP exhibits the largest CPD shift toward 1-hexanol vapours under visible light. The donor–donor characteristics of the molecules may be the cause of their intriguing reaction to 1-hexanol, in addition to intermolecular hydrogen bonding that further supports the enhanced photoresponse behaviour of H_2PyP. Upon exposure to UV light, both H_2PyP and ZnPyP demonstrate n-type characteristics. This phenomenon occurs as the UV light excites electrons from their ground state to higher energy levels, facilitating electron transfer to the conduction band and leading to an accumulation of electrons. The accumulation of electrons results in n-type characteristics in both compounds. On the other hand, on exposure to visible light, H_2PyP exhibits a transition towards p-type characteristics. This transition can be linked to the transfer of electrons induced by light from H_2PyP to

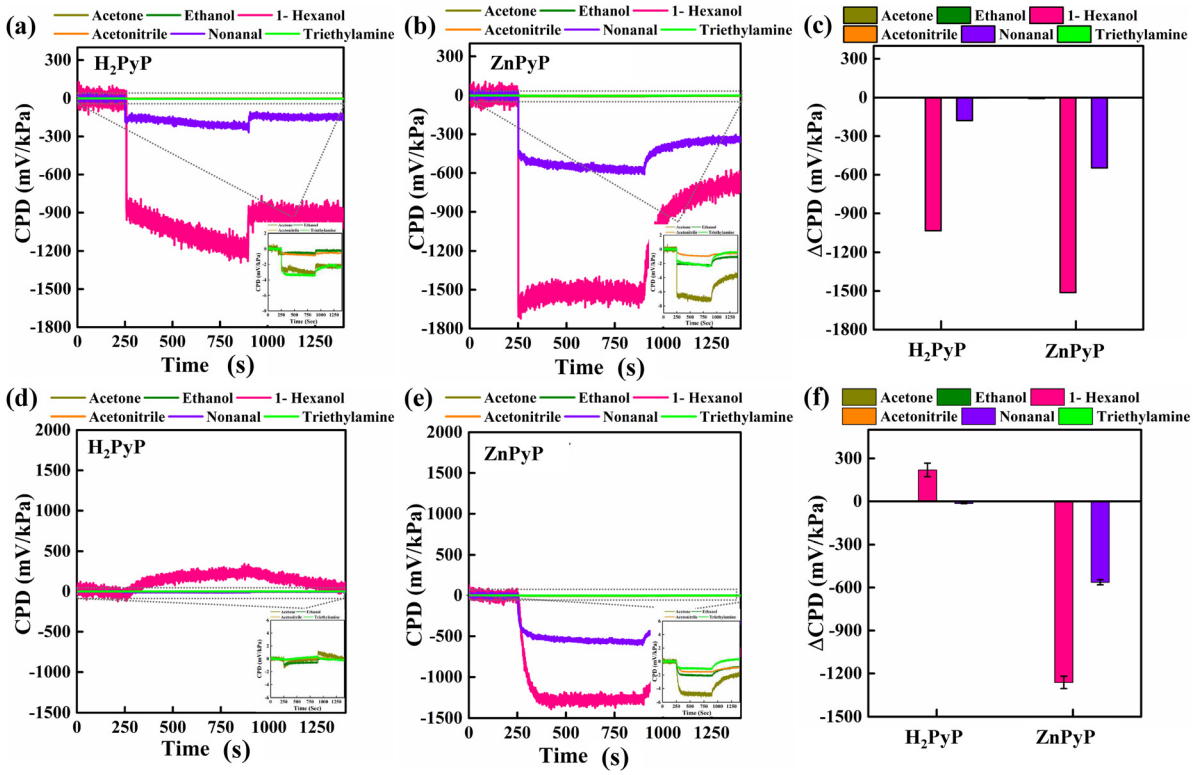

Fig. 5 Single-point CPD plots under UV light illumination for H_2PyP (a) and ZnPyP (b) and under visible light illumination for H_2PyP (d) and ZnPyP (e) with different VOCs. Change in the ΔCPD plots of H_2PyP and ZnPyP under (c) UV and (f) visible light illumination upon VOCs exposure.

its surroundings, leading to the formation of holes within the H_2PyP framework and generating a p-type response. The engagement with particular VOCs, like 1-hexanol, or the intensity of the light source can additionally affect this charge transfer and help stabilize the positive charge generated on the H_2PyP. Additionally, the central Zn metal ion in ZnPyP plays a crucial role in influencing the electronic characteristics of the H_2PyP. The coordination of Zn alters the charge distribution, which may enhance the stability of the system within the n-type region. The maintenance of n-type characteristics in visible light, despite the presence of 1-hexanol, might be attributed to the stabilization of surplus electrons either at the Zn center or within the π-conjugated framework. In contrast, H_2PyP, which does not have metal coordination, lacks the stabilizing effect provided by a central metal ion, rendering it more vulnerable to hole formation. This elucidates the transition to p-type characteristics when exposed to visible light. Consequently, the variations observed between H_2PyP and ZnPyP are mainly influenced by their charge transfer processes in response to varying light conditions, along with the stabilizing impact of Zn coordination.

The difference in the CPD response on exposure to the gases tested, which is supported by UV and visible light, is depicted in Fig. 5(c) and (f) for H_2PyP and ZnPyP, respectively. Of the six VOCs considered, 1-hexanol displayed the highest change in CPD in all modes of light. Both H_2PyP and ZnPyP show greater selectivity towards 1-hexanol exposure followed by nonanal.

Fig. 6 shows 3D raster scan images of H_2PyP and ZnPyP on FTO upon exposure to the 1-hexanol vapours to UV and visible light. The change in the CPD upon exposure to UV light from the dark is illustrated in Fig. 6(a) and (b), which shows a shift in the CPD value from ~ -1500 to ~ 1500 mV kPa^{-1}. A similar shift in the CPD values towards the lower values upon exposure to light is observed in all species. In response to the interaction of H_2PyP and ZnPyP with the concerned gases, a decrease/increase in CPD occurs, which is ascertained due to strong donor (H_2PyP and ZnPyP) donor (1-hexanol) interactions that has occurred through the energy transfer process. From the literature report, the PTL functionalized with MWCNTs under dark and light media exhibited the highest response in the triethylamine vapours due to the presence of pyrene substituted with the carboxylic group at the periphery.[23] Table S2, ESI† summarizes the comparison of different porphyrins and pyrene derivatives employed for the detection of different VOCs. Fig. S11 and S12, ESI† depicts the raster scan images for the interaction of H_2PyP and ZnPyP with various VOCs (ethanol, acetone, acetonitrile, triethylamine, and nonanal) in a dark and light (UV and visible) environment.

Fig. 7 gives the energy level diagrams of ZnPyP under UV and visible light illumination for ambient air and 1-hexanol media. Under the air medium, ZnPyP exhibits a reduced CPD shift from the dark to UV and visible light illumination. Under dark conditions, ZnPyP exhibits a downward band bending under UV light conditions, with the CPD of −175 mV due to the surface depletion barrier caused by adsorbed ionised oxygen and surface states. Conversely, the ZnPyP molecule with a CPD of −344 mV causes downward band bending in the ZnPyP containing 1-hexanol. The photogenerated charge carriers have the ability to excite electrons from the HOMO of ZnPyP to the LUMO level upon UV light irradiation. However, fewer electrons are moved in this way and reach the LUMO, which lowers the electron concentration and increases the resistance. Consequently, a higher upward band is observed. On the other hand, upon exposure to 1-hexanol vapours, 1-hexanol also helps the ZnPyP LUMO by contributing to the electron transition from the HOMO to LUMO triggered by light. Because of its weak attachment to the core carbon atom, the –OH group in 1-hexanol can easily donate electrons to the interfering surface. As a result, there is a higher downward band bending and subsequent increase in the electron concentration on the LUMO, which lowers resistance. Under similar conditions in the dark, ZnPyP exhibits a downward band bending under visible light conditions, with a CPD of −173 mV. This is because of the surface depletion barrier brought on by the surface states and adsorbed ionised oxygen. However, with a CPD of −366 mV, the ZnPyP sample containing 1-hexanol exhibits a downward band bending. The photogenerated charge carriers have the ability to excite electrons from the ZnPyP HOMO level to its LUMO level upon exposure to visible light. However, fewer electrons move in this

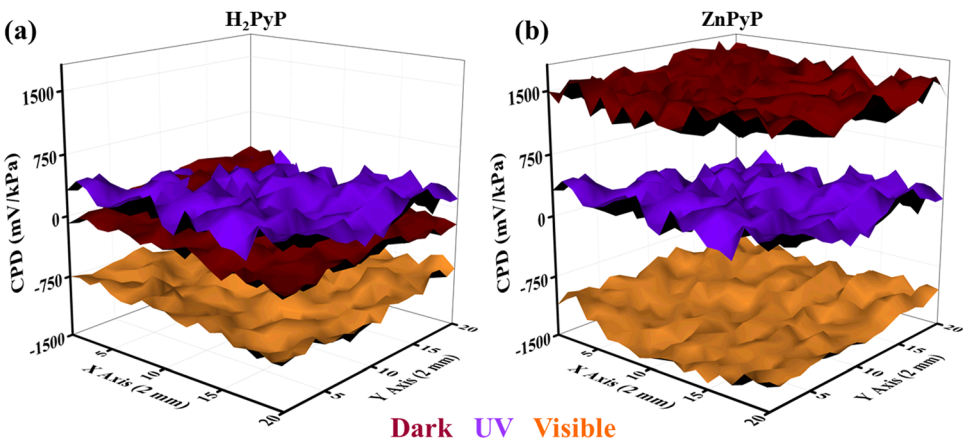

Fig. 6 3D raster scan images of 1-hexanol for (a) H_2PyP and (b) ZnPyP under dark, UV, and visible light illumination.

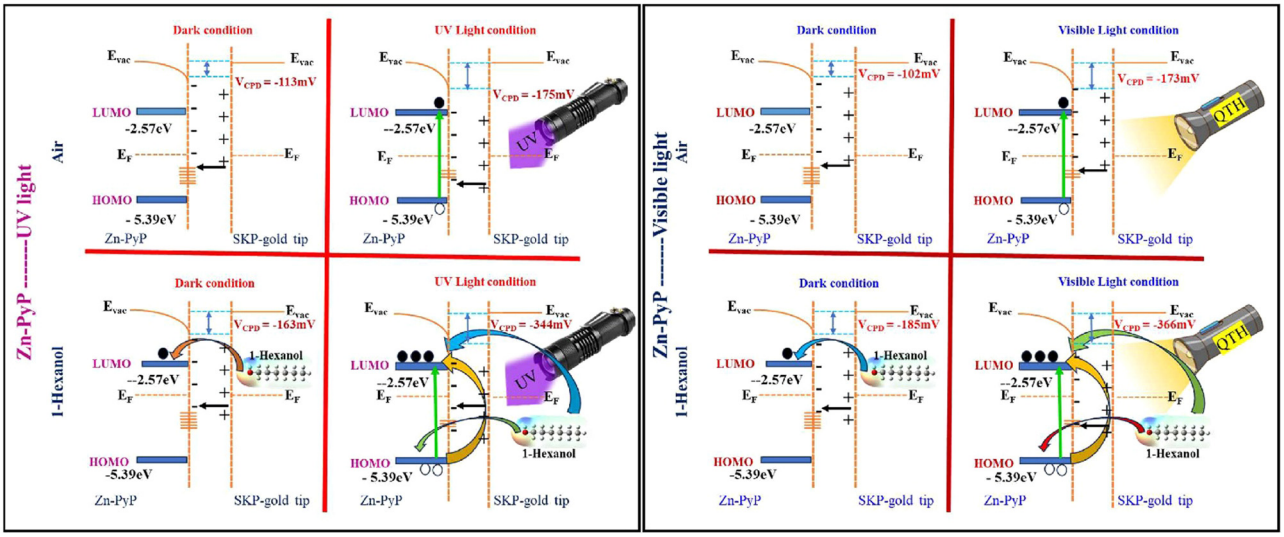

Fig. 7 Schematic of the energy levels of ZnPyP with reference to the gold tip of the SKP instrument under dark, UV and visible light illumination conditions in ambient air and 1-hexanol media.

process and reach the LUMO, which lowers the electron concentration and increases the resistance. Consequently, a higher upward band is observed. On the other hand, when exposed to 1-hexanol vapours, 1-hexanol also helps the ZnPyP LUMO by contributing to electron transition from HOMO to LUMO triggered by light. Because of its weak attachment to the core carbon atom, the –OH group in 1-hexanol is easily able to give electrons to the interfering surface, leading to higher downward band bending and a lowered resistance.

To ascertain the binding interaction between the developed H_2PyP and ZnPyP, the DFT calculations were carried out using the Gaussian16 package with a hybrid exchange–correlation functional B3LYP and basis sets 6-311++G (d,p)/LANL2DZ.[39] Our previous DFT investigations helped in understanding the interaction of different VOCs with various organic molecules to validate the experimental observations.[21–23] The VOCs considered in our study are ethanol, acetone, acetonitrile, 1-hexanol, nonanal, and triethylamine (Fig. S13, ESI†). The H_2PyP, ZnPyP and VOCs structures are modelled and optimized. For the adsorption studies, a complex system containing these organic molecules and VOCs was modelled, and the combined structures were optimized. The adsorption energies (E_{ads}) of the VOCs on the organic sensing molecules were calculated using the formula,

$$E_{ads} = E_{(organic\ molecule+VOC)} - E_{(organic\ molecule)} - E_{VOC} \quad (4)$$

where $E_{(organic\ molecule+VOC)}$, $E_{(organic\ molecule)}$ and E_{VOC} are the total energies of the complex molecule, organic molecule and VOCs, respectively.[25] The charge transfer between the organic molecules and VOCs was calculated using the Mulliken charge analysis.

The optimized structures of H_2PyP and ZnPyP, along with their electrostatic potential (ESP) plots, are shown in Fig. 8 and Table 2. The red and blue regions in the ESP plot indicate the electron-rich and deficient regions. From the ESP plots, it is clear that the central core is the active site for VOC interactions. Thus, the VOCs will interact more with the porphyrin core rather than the pyrene group, even though the pyrene group acts as an additional active site. The HOMO–LUMO values of the organic

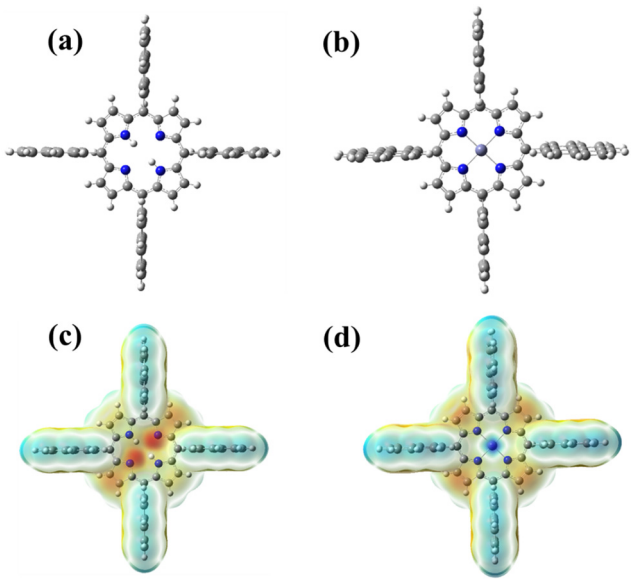

Fig. 8 Molecular structures of (a) H_2PyP and (b) ZnPyP; ESP plots of (c) H_2PyP and (d) ZnPyP.

Table 2 Electronic properties of the organic molecules and VOCs

Molecule	HOMO (eV)	LUMO (eV)	Energy gap (eV)
H_2PyP	−5.39	−2.62	2.77
ZnPyP	−5.42	−2.56	2.86
Ethanol	−7.67	−0.36	7.31
Acetone	−7.05	−0.77	6.28
Acetonitrile	−9.26	−0.57	8.69
1-Hexanol	−7.55	−0.33	7.22
Nonanal	−7.19	−0.98	6.21
Triethylamine	−5.86	−0.16	5.70

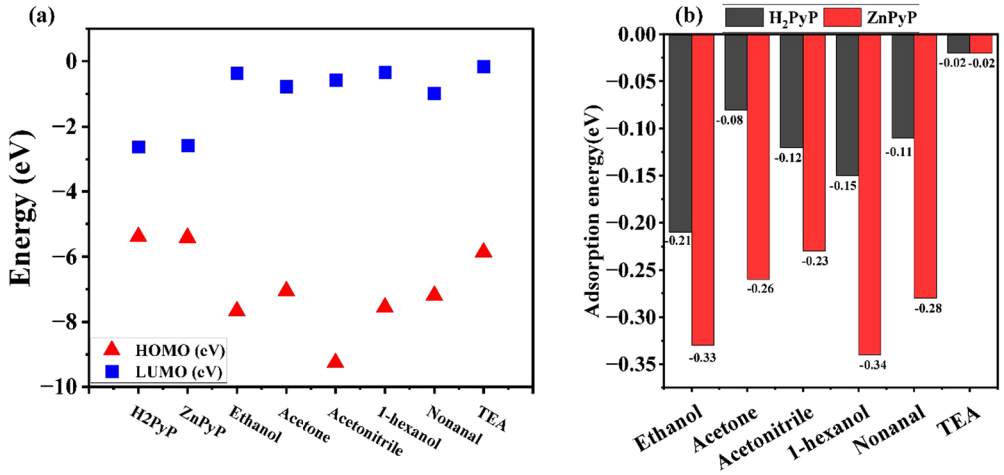

Fig. 9 (a) HOMO–LUMO values of H_2PyP, ZnPyP and VOCs. (b) Adsorption energy of VOCs with H_2PyP and ZnPyP.

molecules and VOCs are mapped, as shown in Fig. 9(a). The metalation led to a small change in the energy gap.

The VOCs interacted with the central core as well as the peripheral ring of the organic molecules. It is found that VOCs show higher interaction with the porphyrin core. The central core site is more favourable compared to the peripheral site since a higher adsorption energy was obtained at the central core site, which is in agreement with the similar procedure reported on the porphyrin system containing triphenylamine.[40] The adsorption energies of VOCs with the organic molecules are represented in Fig. 9(b). The obtained energy values are in the range of −0.33 eV to −0.02 eV. As the magnitude of the adsorption energy range is less than −1 eV during the interaction of VOCs with H_2PyP and ZnPyP, it results in a favourable physisorption process. However, this kind of adsorption energy range aligns with the earlier observations.[41] This confirms that all interactions are physisorption in nature. In all the cases, the VOCs interacted more with ZnPyP than H_2PyP, and thus, the central metal played a vital role in the adsorption. The introduction of a metal improves the VOC adsorption property. Interestingly, both H_2PyP and ZnPyP molecules show higher interaction towards VOCs belonging to the alcohol family, particularly 1-hexanol, ethanol followed by nonanal, acetone and acetonitrile. The details on the adsorption energy of VOCs with H_2PyP and ZnPyP molecules are provided in Tables S3 and S4 in ESI.† The Mulliken charge transfer between the organic molecules and VOCs is shown in (Fig. S14, ESI†). A significant charge transfer occurred between nonanal and the organic molecules. The computational results confirm that both H_2PyP and ZnPyP have more affinity towards alcohols, especially towards 1-hexanol, compared to other VOCs.

4. Conclusions

In summary, we developed a freebase porphyrin and its Zn(II) complex with orthogonally oriented pyrene units at the meso position, and thin films were obtained. The combined photophysical studies reveal that appreciable electronic interaction occurs between the porphyrin π-system and the meso-substituted pyrene units. The photophysical studies exhibited that the energy-transfer process is highly predominant with long-lived charge-separated states attributed to the delocalization of the porphyrin to the pyrene units, acting as strong donor compounds. The gas adsorption studies of H_2PyP and ZnPyP with different VOCs indicated good sensitivity and selectivity towards the detection of 1-hexanol vapours upon exposure to UV and visible light conditions. Under UV light conditions, both H_2PyP and ZnPyP showed an n-type behaviour while H_2PyP exhibited a p-type and ZnPyP showed an n-type behaviour under visible light towards 1-hexanol. H_2PyP demonstrates a significant photovoltage response of 93% within 17 seconds of exposure, accompanied by a recovery rate of 23% over 5 seconds. In contrast, ZnPyP exhibits an even higher photovoltage response of 97% in just 2 seconds, with a recovery rate of 55% achieved within 116 seconds under UV light. ZnPyP exhibits superior response and recovery times than H_2PyP due to variations in the mode of intermolecular interactions through the metal centre and an efficient photoinduced energy transfer process. The surface binding studies through DFT calculations confirm the strong photoresponse of the porphyrin derivatives to 1-hexanol, consistent with experimental data. Fine-tuning the structure–property correlation and design strategy could be useful for developing dual-mode light-assisted chemical sensing field-effect transistors and new sensing platforms for detecting alcohols in food and the environment.

Author contributions

All authors contributed to the study. In particular: Prasanth Palanisamy: writing–original draft, methodology, investigation, formal analysis, conceptualization. Mageshwari Anandan: writing – original draft methodology, investigation, formal analysis and validation. Sheethal Sasi: methodology, investigation, formal analysis and validation. Arbacheena Bora: investigation, formal analysis and validation. Sarath Kumar Chedharla Balaji: investigation, formal analysis and validation. Rence P. Reji: investigation, formal analysis and validation. Yoshiyuki Kawazoe:

supervision, resources. Kommineni Kalyani: morphology, investigation, formal analysis and Validation. Surya Velappa Jayaraman: writing–review & editing, supervision, resources and funding acquisition. Yuvaraj Sivalingam: supervision, resources and funding acquisition. Venkatramaiah Nutalapati: concept, writing – review & editing, supervision, resources and funding acquisition.

Data availability

The data that support the findings of this study are available from the corresponding author upon reasonable request. Details related to the structural characterization (NMR, mass and FT-IR), emission spectra and SKP measurements are provided in the ESI.†

Conflicts of interest

The authors declare that they have no known competing financial interests or personal relationships that could have appeared to influence the work reported in this paper.

Acknowledgements

NVR greatly acknowledges the Science & Engineering Research Board (SERB), Government of India, for funding through a start-up research grant (SRG/2019/001023), Central Power Research Institute (CPRI, a Government of India society under the Ministry of Power) for funding through the R&D project (CPRI/R&D/TC/GDEC/2022) and the SRMIST seed grant. Y. S. and V. J. S. thank DST-SERB for the financial support under the Core Research Grant (CRG/2021/006647). The authors also acknowledge the Photoluminescence spectrometer facility, NRC, and SCIF of SRMIST for analytical characterization. The authors would like to express their sincere thanks to the crew of the Center for Computational Materials Science at the Institute for Materials Research, Tohoku University, for their continuous support of supercomputing facilities. Additionally, the authors thank SRM-HPCC for providing access to the supercomputer for computations. PP and MA thank SRMIST for the PhD fellowship.

References

1 E. David and V. C. Niculescu, *Int. J. Environ. Res. Public Health*, 2021, **18**, 13147.
2 B. P. Singh, S. S. Sohrab, M. Athar, T. A. Alandijany, S. Kumari, A. Nair, S. Kumari, K. Mehra, K. Chowdhary, S. Rahman and E. I. Azhar, *Toxics*, 2023, **11**, 165.
3 R. Epping and M. Koch, *Molecules*, 2023, **28**, 1598.
4 S. Giannoukos, B. Brkić, S. Taylor, A. Marshall and G. F. Verbeck, *Chem. Rev.*, 2016, **116**, 8146–8172.
5 M. R. Miah, M. Yang, S. Khandaker, M. M. Bashar, A. K. D. Alsukaibi, H. M. A. Hassan, H. Znad and M. R. Awual, *Sens. Actuators, A*, 2022, **347**, 113933.
6 J. Iglesias, I. Medina, F. Bianchi, M. Careri, A. Mangia and M. Musci, *Food Chem.*, 2009, **115**, 1473–1478.
7 R. Podduturi, G. da Silva David, R. J. da Silva, G. Hyldig, N. O. G. Jørgensen and M. Agerlin Petersen, *Food Res. Int.*, 2023, **173**, 113375.
8 L. Makhlouf, K. El Fakhouri, S. A. Kemal, A. Aasfar, I. Meftah Kadmiri and M. El Bouhssini, *Front. Hortic.*, 2024, **3**, 1–12.
9 A. Nazarov and D. Thierry, *Front. Mater.*, 2019, **6**, 1–17.
10 A. Schütze, T. Baur, M. Leidinger, W. Reimringer, R. Jung, T. Conrad and T. Sauerwald, *Environments*, 2017, **4**, 1–13.
11 P. Hajivand, J. Carolus Jansen, E. Pardo, D. Armentano, T. F. Mastropietro and A. Azadmehr, *Coord. Chem. Rev.*, 2024, **501**, 215558.
12 Y. A. Waghmare, V. N. Narwade, A. Umar, A. A. Ibrahim and M. D. Shirsat, *Chem. Phys. Impact*, 2024, **8**, 100419.
13 S. Supriya, V. S. Shetti and G. Hegde, *New J. Chem.*, 2018, **42**, 12328–12348.
14 N. Nath, A. Kumar, S. Chakroborty, S. Soren, A. Barik, K. Pal and F. G. de Souza, *ACS Omega*, 2023, **8**, 4436–4452.
15 A. D. F. Dunbar, S. Brittle, T. H. Richardson, J. Hutchinson and C. A. Hunter, *J. Phys. Chem. B*, 2010, **114**, 11697–11702.
16 A. D. Rushi, K. P. Datta, P. Ghosh, A. Mulchandani and M. D. Shirsat, *Sens. Actuators, B*, 2018, **257**, 389–397.
17 R. Paolesse, S. Nardis, D. Monti, M. Stefanelli and C. Di Natale, *Chem. Rev.*, 2017, **117**, 2517–2583.
18 Z. Li, C. J. Zeman, S. Valandro, J. P. O. Bantang and K. S. Schanze, *Molecules*, 2023, **28**, 4115.
19 S. Hiroto, Y. Miyake and H. Shinokubo, *Chem. Rev.*, 2017, **117**, 2910–3043.
20 G. Magna, M. Muduganti, M. Stefanelli, Y. Sivalingam, F. Zurlo, E. Di Bartolomeo, A. Catini, E. Martinelli, R. Paolesse and C. Di Natale, *ACS Appl. Nano Mater.*, 2021, **4**, 414–424.
21 G. Marappan, K. Pushparaj, Y. Sivalingam, V. Nutalapati and V. J. Surya, *Mater. Lett.*, 2021, **304**, 130724.
22 K. Selvaraj, G. Marappan, P. Gawas, S. Raviteja, G. Dinesh Kumar, V. Jayaraman Surya, Y. Sivalingam and V. Nutalapati, *Mater. Lett.*, 2021, **303**, 2–5.
23 M. Elakia, M. Gobinath, Y. Sivalingam, E. Palani, S. Ghosh, V. Nutalapati and V. J. Surya, *Phys. E*, 2020, **124**, 114232.
24 Y. Sivalingam, G. Magna, R. Kalidoss, S. Murugan, D. Chidambaram, V. Nutalapati, S. V. Jayaraman, R. Paolesse and C. D. Natale, *Nanotechnology*, 2022, **33**, 075503.
25 R. P. Reji, G. Marappan, Y. Sivalingam and V. Jayaraman Surya, *Mater. Lett.*, 2022, **306**, 130945.
26 X. Wang, S. Li, L. Zhao, C. Xu and J. Gao, *Chin. J. Chem. Eng.*, 2020, **28**, 532–540.
27 P. P. Gawas, A. Bora, R. P. Reji, B. Ramakrishna, P. B. Managutti, C. R. Göb, S. Mohamed, Y. Kawazoe, S. Velappa Jayaraman, Y. Sivalingam and V. Nutalapati, *J. Phys. Chem. C*, 2023, **127**, 6466–6482.
28 P. P. Gawas, A. Bora, R. P. Reji, S. K. Cb, B. Ramakrishna, V. Nalluri, S. V. Jayaraman, Y. Sivalingam and V. Nutalapati, *ACS Appl. Electron. Mater.*, 2022, **4**, 2313–2325.
29 S. Sasi, G. Marappan, Y. Sivalingam, M. Chandran, G. Magna, S. Velappa Jayaraman, R. Paolesse and C. Di Natale, *Surf. Interfaces*, 2024, **50**, 104456.

30 G. Marappan, A. K. Mia, K. Puspharaj, S. Vaidyanathan, Y. Kawazoe, Y. Sivalingam and V. J. Surya, *Surf. Interfaces*, 2024, **44**, 103648.
31 T. Zoltan, F. Vargas, C. Rivas, V. López, J. Perez and A. Biasutto, *Sci. Pharm.*, 2010, **78**, 767–790.
32 T. M. Halasinski, F. Salama and L. J. Allamandola, *Astrophys. J.*, 2005, **628**, 555–566.
33 Y. Okabe, S. K. Lee, M. Kondo and S. Masaoka, *JBIC, J. Biol. Inorg. Chem.*, 2017, **22**, 713–725.
34 M. Managa, J. Britton, E. K. Amuhaya and T. Nyokong, *J. Lumin.*, 2017, **185**, 34–41.
35 N. S. Ramgir, P. K. Sharma, N. Datta, M. Kaur, A. K. Debnath, D. K. Aswal and S. K. Gupta, *Sens. Actuators, B*, 2013, **186**, 718–726.
36 Y. Sivalingam, P. Elumalai, S. V. J. Yuvaraj, G. Magna, V. J. Sowmya, R. Paolesse, K. W. Chi, Y. Kawazoe and C. Di Natale, *J. Photochem. Photobiol., A*, 2016, **324**, 62–69.
37 Y. Sivalingam, E. Martinelli, A. Catini, G. Magna, G. Pomarico, F. Basoli, R. Paolesse and C. Di Natale, *J. Phys. Chem. C*, 2012, **116**, 9151–9157.
38 G. Marappan, R. P. Reji, V. Mohan, T. V. L. Kumar, Y. Sivalingam and V. J. Surya, *J. Mater. Sci.: Mater. Electron.*, 2022, **33**, 9590–9598.
39 M. J. Frisch, G. W. Trucks, H. B. Schlegel, G. E. Scuseria, M. A. Robb, J. R. Cheeseman, G. Scalmani, V. Barone, G. A. Petersson and H. Nakatsuji, *Gaussian 16*, Gaussian. Inc., Wallingford CT, 2016.
40 P. Palanisamy, M. Anandan, S. Sasi, A. Bora, R. P. Reji, C. B. S. Kumar, Y. Kawazoe, G. Raman, S. V. Jayaraman and Y. Sivalingam, *Sustainable Mater. Technol.*, 2025, e01239.
41 C. B. S. Kumar, R. P. Reji, Y. Sivalingam, Y. Kawazoe and V. J. Surya, *RSC Adv.*, 2024, **14**, 28182–28200.